Appl Biochem Biotechnol (2009) 158:445–456
DOI 10.1007/s12010-008-8415-9

# Intensification of Biocatalytical Processes by Synergistic Substrate Conversion. Fungal Peroxidase Catalyzed *N*-Hydroxy Derivative Oxidation in Presence of 10-Propyl Sulfonic Acid Phenoxazine

**Juozas Kulys · Zilvinas Dapkunas · Robert Stupak**

Received: 4 June 2008 / Accepted: 27 October 2008 /
Published online: 18 November 2008


**Abstract** Many industrial pollutants, xenobiotics, and industry-important compounds are known to be oxidized by peroxidases. It has been shown that highly efficient peroxidase substrates are able to enhance the oxidation of low reactive substrate by acting as mediators. To explore this effect, the oxidation of two *N*-hydroxy derivatives, i.e., *N*-hydroxy-*N*-phenyl-acetamide (HPA) and *N*-hydroxy-*N*-phenyl-carbamic acid methyl ester (HPCM) catalyzed by recombinant *Coprinus cinereus* (rCiP) peroxidase has been studied in presence of efficient substrate 3-(4a,10a-dihydro- phenoxazin-10-yl)-propane-1-sulfonic acid (PPSA) at pH 8.5. The bimolecular constant of PPSA cation radical reaction with HPA was estimated to be $(2.5\pm 0.2)\cdot 10^7$ $M^{-1}$ $s^{-1}$ and for HPCM was even higher. The kinetic measurements show that rCiP-catalyzed oxidation of HPA and HPCM can increase up to 33,000 times and 5,500 times in the presence of equivalent concentration of high reactive substrate PPSA. The mathematical model of synergistic rCiP-catalyzed HPA–PPSA and HPCM–PPSA oxidation was proposed. Experimentally obtained rate constants were in good agreement with those calculated from the model confirming the synergistic scheme of the substrate oxidation. In order to explain the different reactivity of substrates, the docking of substrates in the active site of the enzyme was calculated. Molecular dynamic calculations show that the enzyme–substrate complexes are structurally stable. The high reactive PPSA exhibited higher affinity to enzyme active site than HPA and HPCM. Furthermore, the orientation of HPA and HPCM was not favorable for proton transfer to the distal histidine, and different substrate reactivity was explained by these diversities.

**Keywords** Synergistic · *Coprinus cinereus* peroxidase · *N*-hydroxy derivative · 3-(4a,10a-dihydro- phenoxazin-10-yl)-propane-1-sulfonic acid · Kinetics · Docking modeling · Molecular dynamics

**Abbreviations**

| | |
|---|---|
| HPA | *N*-hydroxy-*N*-phenyl-acetamide |
| HPCM | *N*-hydroxy-*N*-phenyl-carbamic acid methyl ester |

J. Kulys (✉) · Z. Dapkunas · R. Stupak
Faculty of Fundamental Sciences, Department of Chemistry and Bioengineering,
Vilnius Gediminas Technical University, Sauletekio Avenue 11, 10223 Vilnius, Lithuania
e-mail: Juozas.Kulys@fm.vgtu.lt

| | |
|---|---|
| rCiP | recombinant *Coprinus cinereus* peroxidase |
| ARP I/II | *Arthromyces ramosus* peroxidase compound I and II |
| PPSA | 3-(4a,10a-dihydro- phenoxazin-10-yl)-propane-1-sulfonic acid |
| TEMPO | 2,2,6,6-tetramethyl-piperidine-1-oxyl radical |

## Introduction

The heme-containing peroxidases are known to catalyze the oxidation of a wide range of structurally diverse aromatic compounds. It is well established that oxidation of substrates occurs with two one-electron transfer reactions through the enzyme compound I and compound II formation. The oxidation of substrates leads to free-radical intermediates [1], which are known to participate in a variety of nonenzymic reactions including disproportionation, polymerization, and electron transfer [2–4].

It has been shown that highly efficient peroxidase substrates are able to enhance the oxidation of low reactive substrate. This synergistic effect can be attributed to the formation of short-lived cation radicals or other oxidized states of highly efficient substrate, which participate in the oxidation of the low reactive substrate.

The stimulation of laccase-catalyzed N-OH derivative (TEMPO) oxidation by highly reactive substrate 3-(4a,10a-dihydro- phenoxazin-10-yl)-propane-1-sulfonic acid (PPSA) was investigated very recently. It was shown that the reaction rate increases more than 500 times if PPSA is used [5]. Such effect for peroxidase-catalyzed aminopyrine oxidation by various phenothiazines was demonstrated, too [6]. Thus, the stimulation of biocatalytic processes using highly reactive substrates opens new possibilities of enzyme catalysis exploitation. Under these circumstances, it is important examine the mechanism of such synergistic processes which can be applied to build efficient coenzyme-regenerating systems or highly sensitive biosensors.

One reaction catalyzed by peroxidases that may be affected by redox mediation is the oxidation of *N*-hydroxy derivatives. *N*-hydroxy derivatives introduced by *Call and Mucke* [7] have been suggested as mediators in peroxidase- and laccase-catalyzed dye and lignin bleaching as well as lignin degradation. These compounds were used as mediators for laccase-catalyzed phenol [8] and polycyclic aromatic hydrocarbon degradation [9]. However, the oxidation of N-OH compounds by peroxidase and laccase is relatively slow [10, 11]. Such reactivity was explained by low proton transfer rate in the active site of the peroxidase and laccase [12, 13].

To elucidate the reaction mechanism, various analyses of *Arthromyces ramosus* peroxidase (ARP) complexes with N-OH compounds were performed. Analysis of the salicylhydroxamic and benzhydroxamic acid and ARP revealed that, upon binding of N-OH compounds, the peroxidase partially converts to a six-coordinated heme [14]. The N-OH compound aromatic ring binds to the hydrophobic region at the opening of the active site and the hydroxamic acid moiety forms hydrogen bonds with the active site amino acid histidine (His), arginine (Arg), and proline (Pro) and is not associated with heme iron [15, 16]. However, how substrate arrangement in the active site can effect reactivity is unclear.

The present paper demonstrates synergistic oxidation of N-OH derivatives *N*-hydroxy-*N*-phenyl-acetamide (HPA) and *N*-hydroxy-*N*-phenyl-carbamic acid methyl ester (HPCM) using 3-(4a,10a-dihydro- phenoxazin-10-yl)-propane-1-sulfonic acid (PPSA; Fig. 1). Mathematical model for this process was proposed. Furthermore, the reactivity of HPA, HPCM, and PPSA was explained by their arrangement diversities in active site of peroxidase.

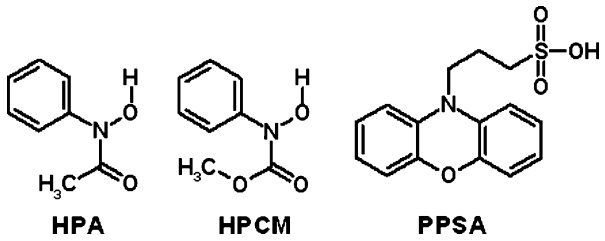


**Fig. 1** Structure of investigated compounds. *N*-hydroxy-*N*-phenyl-acetamide (*HPA*), *N*-hydroxy-*N*-phenyl-carbamic acid methyl ester (*HPCM*), 3-(4a,10a-dihydro-phenoxazin-10-yl)-propane-1-sulfonic acid (*PPSA*)

## Materials and Methods

### Reagents

The recombinant *Coprinus cinereus* peroxidase (rCiP) was additionally purified by anion exchange chromatography and provided by Novo Nordisk A/S (Denmark). It was homogenous as assessed by sodium dodecyl sulfate polyacrylamide gel electrophoresis. The concentration of rCiP was determined spectrophotometrically at 405 nm using an extinction coefficient of $1.08 \cdot 10^5$ $M^{-1}$ $cm^{-1}$ [1]. The solutions of $H_2O_2$ were prepared from 30% stock and concentrations were determined at 230 nm using an extinction coefficient of 72.4 $M^{-1}$ $cm^{-1}$. HPA, HPCM, and PPSA were used as received from Novo Nordisk A/S (Denmark). The solutions of HPA and HPCM were prepared by weight in deionized water ($R$>18.2 M Ω). The PPSA concentration was determined spectrophotometrically by monitoring long-term cation radical ($PPSA^{\cdot+}$) formation at 525 nm using an extinction coefficient of 9,500 $M^{-1}$ $cm^{-1}$ [17].

### Kinetic Measurements

The steady-state kinetics of HPA and HPCM oxidation was monitored using the computer-assisted Ultrospec JJ LKB UV/Visible spectrophotometer. Initial rates of HPA and HPCM oxidation in the presence and absence of PPSA were monitored at 310 nm ($\varepsilon_{310}$=8,900 $M^{-1}$ $cm^{-1}$) [10] and 307 nm ($\Delta\varepsilon_{307}$=4,900 $M^{-1}$ $cm^{-1}$) [11], respectively. The measurements were carried out at 25± 0.1 °C in 20-mM Tris–HCl buffer solution (pH 8.5). Reaction mixture contained 2–240 nM rCiP, 0.1 mM $H_2O_2$, 1–60 μM HPCM, 1–60 μM HPA, and 0.5–4 nM PPSA. All reactions were initiated by the addition of enzyme to reaction mixture. No oxidation reaction occurred without an enzyme.

The rate constants of $PPSA^{\cdot+}$ reduction by HPA and HPCM were determined using computer-assisted stop-flow spectrophotometer Otsuka RA-401 (Japan). Delay time was set to 15 ms and the progress of the reaction was monitored for 10 ms. The measurements were carried out at 25±0.1 °C in 20-mM Tris–HCl buffer solution (pH 8.5). Reaction mixture contained ≤17 μM $PPSA^{\cdot+}$ and 3–10 μM HPA. The solutions of $PPSA^{\cdot+}$ were prepared in 20-mM sodium phosphate buffer (pH 7) using 14 nM rCiP peroxidase, 0.25 mM $H_2O_2$, and 0.2 mM PPSA. After conversion of PPSA to cation radical, rCiP was inactivated by removing the $H_2O_2$ by the addition 3.6 nM of *Aspergillus niger* catalase. Thus, the rCiP was inactive in further reactions. Further, the obtained $PPSA^{\cdot+}$ solution was mixed with HPA and HPCM solutions. The progress of the reaction was monitored according to $PPSA^{\cdot+}$ absorption at 525 nm.

## Data Analysis and Calculations

The fitting of steady-state kinetic data was performed using GRAFIT 3.01 software package. Kinetic data for HPA were approached by single exponential function and initial rate was calculated according to Eq. 1.

$$V_{\text{init}} = k \cdot A_{\infty}/\varepsilon \tag{1}$$

Since the absorbance of HPCM overlapped with the absorbance of its oxidation product, the initial rate was calculated according to Eq. 2.

$$V_{\text{init}} = k \cdot (A_{\infty} - A_0)/\Delta\varepsilon \tag{2}$$

The calculated initial reaction rate was used for further analysis. If the initial rate was a linear function of substrate concentration, an apparent bimolecular rate constant was calculated from its slope. If the rate showed a saturating character, an apparent Michaelis constant ($K_{\text{m}}$) and a catalytic constant ($k_{\text{cat}}$) was calculated according to Michaelis–Menten equation. In this case, an apparent bimolecular rate constant ($k_{\text{ox}}$) was defined as $k_{\text{cat}}/K_{\text{m}}$.

To determine the rate constant (k12) of $PPSA^{\bullet+}$ reduction by HPA and HPCM, kinetic curves of $PPSA^{\bullet+}$ concentration were analyzed by applying bimolecular reaction scheme 3 with the establishment of equilibrium:

$$\text{PPSA}^{\cdot+} + \text{S} \underset{k_{21}}{\overset{k_{12}}{\leftrightarrow}} \text{PPSA} + \text{P} \tag{3}$$

where $PPSA^{\bullet+}$/PPSA and S/P correspond to the oxidized and reduced forms of PPSA and *N*-hydroxy compounds, respectively. $k_{12}$ and $k_{21}$ are the bimolecular rate constants of $PPSA^{\bullet+}$ reaction with reduced *N*-hydroxy compounds and PPSA reaction with oxidized *N*-hydroxy compounds, respectively. The experimental curves of $PPSA^{\bullet+}$ concentration were fitted to integral equation which was derived from the reaction scheme using a symbolic operator of MathcadPro 2001.

The self-exchange rate constant ($k_{11}$) for HPA was calculated according to the outer-sphere electron transfer theory [18]:

$$k_{12} = (k_{11} \cdot k_{22} \cdot K_{12} \cdot f_k)^{1/2} \tag{4}$$

$$\log(f_k) = \log(K_{12})^2 \Big/ 4 \cdot \log\left(k_{11} \cdot k_{22} \cdot Z^2\right) \tag{5}$$

where $Z$ is the collision frequency (taken to be $10^{11}$ $M^{-1}$ $s^{-1}$ at 25 °C); $K_{12}$ is the equilibrium constant; $k_{22}$ is the self-exchange reaction rate constant of PPSA. $K_{12}$ was calculated from the reactant redox potential difference ($\Delta E(V) = E_{\text{PPSA}} - E_{\text{HPA}}$):

$$\ln(K_{12}) = (\Delta E \cdot n \cdot F)/(R \cdot T) \tag{6}$$

where $n$ is the number of electrons; $F$ is the Faraday constant; $R$ is the universal gas constant and $T$ is the temperature. The value of $k_{22}$ for PPSA is assumed to be $2.2 \cdot 10^9$ $M^{-1}$ $s^{-1}$ [19] and redox potentials of HPA, HPCM, and PPSA are 0.611 V [10], 0.586 V [11], and 0.623 V [5] versus NHE, respectively.

The data are presented as mean values±standard deviation. The expression of initial steady-state rate for the synergistic scheme was built using symbolic algebra of MathCAD 2001 Pro software package.

### *Ab initio*, Docking, and Molecular Dynamics Calculations

The calculations of HPA, HPCM, and dissociated form of PPSA structures and partial atomic charges were performed using Gaussian 98-W package [20]. The optimization of substrate geometry was accomplished using HF/3–21G basis set. The optimized geometry of molecules was used for partial atomic charges calculation with the HF/6–31G basis set.

The simulations of substrate docking in the active site of enzyme were performed with Auto Dock 3.0 [21–23]. The structure of ARP that has in addition one terminal amino group in comparison to recombinant *C. cinereus* peroxidase [24] was chosen. The crystal data of ARP (PDB-ID: 1ARP) with resolution of 1.9 Å were downloaded from the Protein Data Bank. All water molecules were removed, except the oxygen atom of one structural water molecule that was left at the distal side of heme in the active site of ARP. In order to model the catalytically active state of ARP, i.e., compound I/II, the distance of Fe=O bond was set to 1.77 Å, i.e., the average Fe=O distance of compounds I and II of horseradish peroxidase [25].

The energy grid maps of atomic interaction were calculated with 0.15-Å grid spacing and 120 grid points forming an 18-Å cubic box cantered at the active site of peroxidase. The docking was accomplished using the Lamarkian genetic algorithm [21]. The number of individuals in populations was set to 50. The maximum number of evaluations of this algorithm was 2,500,000; maximum number performed was 27,000.

Molecular dynamics (MD) simulations were performed with GROMACS 3.2.1 package [26, 27]. GROMOS-96 43a1 force field (FF) was used [28]. Modeled geometries of HPA, HPCM, and PPSA and peroxidase complexes containing the lowest substrates docking energies where supplied for MD simulations. The topologies for HPA, HPCM, and PPSA (dissociated form) were generated with PRODRG2 server [29]. The topology of ARP I/II oxidative form was generated using pbd2gmx program [26, 27].

The enzyme–substrate complexes were dissolved in Simple-Point-Charge-type water solvent [30]. Total negative charge of modeled systems was neutralized with sodium ions. The modeled systems were energy-minimized using the steepest descent method with no constrains. Further, such structures were supplied to 50-ps position-restrained dynamics, where lengths of all bonds were constrained with LINCS algorithm [31]. Berendsen temperature and pressure coupling scheme was used [32]. During the position-restrained dynamics calculations, the temperature was maintained close to 300°K and the pressure was 1 bar. Particle-Mesh Ewald scheme [33] was used to treat nonbonded electrostatics and twin range cutoff scheme was used for nonbonded Lennard-Jones (LJ) treatment. The long-range cutoff was set at 1.0 and 1.0 nm for electrostatics and LJ. System atoms were supplied with velocities generated with Maxwellian distribution. Five-hundred-picosecond MD simulations with no constrains were performed on the structures obtained after position-restrained dynamics with the same option described above about position-restrained dynamics.

## Results and Discussion

### Reactivity of HPA, HPCM, and PPSA

The kinetics of HPA and HPCM oxidation was investigated in the presence of hydrogen peroxide and rCiP at pH 8.5. The initial oxidation rates of HPA and HPCM in the absence of PPSA were proportional to the enzyme concentration (Fig. 2). Initial oxidation rate increased up to 12.5 nM $s^{-1}$ and 73 nM $s^{-1}$ at 240 nM of rCiP, for HPA and HPCM, respectively.

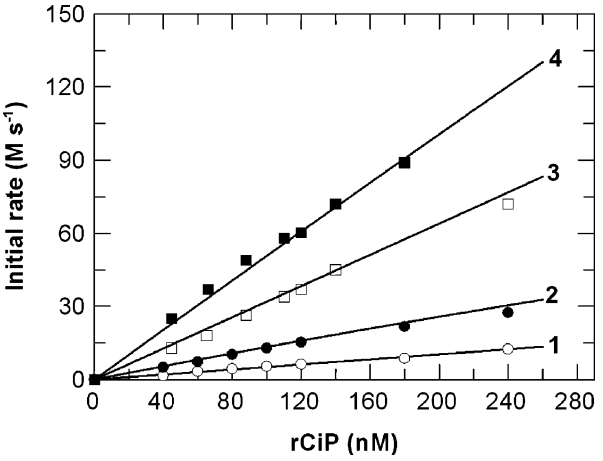


**Fig. 2** The dependence of HPA and HPCM initial oxidation rate on rCiP concentration, at pH 8.5, 25 °C, 0.1 mM $H_2O_2$: (*1*) 20 μM HPA without PPSA, (*2*) 20 μM HPA with 3.4 nM PPSA, (*3*) 20 μM HPCM without PPSA, (*4*) 20 μM HPCM with 3.4 nM PPSA. Curves are the result of data fitting with a model

The dependence of initial oxidation rate on substrate concentrations was linear. The initial rate increased up to 11.3 and 21.4 nM $s^{-1}$ at 60 μM of HPA and HPCM, respectively (Fig. 3). According to the results calculated, apparent bimolecular constants were (2.4±0.2)·$10^3$ $M^{-1}$ $s^{-1}$ and (1.4±0.2)·$10^4$ $M^{-1}$ $s^{-1}$ for HPA and HPCM, respectively. The established values were in good agreement with those reported in [10, 11].

The oxidation of various PPSA concentrations exhibited saturation kinetics (data not shown). The apparent bimolecular rate constant was calculated according to $k_{app} = V_{max}/(K_m \cdot [rCiP])$ using estimated parameters $V_{max}$=(301.2±10.1) nM/s and $K_m$=(22.2±2.5) μM and it was (9.7±0.4)·$10^7$ $M^{-1}$ $s^{-1}$.

The peroxidase-catalyzed oxidation of HPA and HPCM stimulated to a great extent in the presence of PPSA. The initial oxidation rate of HPA and HPCM was linearly dependant on rCiP concentration and increased up to 28 and 141 nM $s^{-1}$ in the presence of 3.4 nM of PPSA, respectively (Fig. 2). The largest increase was observed at the least enzyme concentration.

The initial oxidation rate of various HPA and HPCM concentrations in the presence of 3.4 nM PPSA increased up to 26 and 120 nM $s^{-1}$ at 60 μM of HPA and HPCM, respectively (Fig. 3). The largest increase was observed at the least HPA and HPCM concentrations.

The dependence of initial oxidation rate of HPA and HPCM on PPSA concentration was linear (Fig. 4). The initial rate of HPA oxidation increased from 4 nM $s^{-1}$ in the absence of PPSA up to 14 nM $s^{-1}$ at the presence of 6.7 nM of PPSA (Fig. 4). Similar results were obtained for HPCM; the initial rate of HPCM increased from 20 nM $s^{-1}$ in the absence of PPSA up to 35 nM $s^{-1}$ at 6.7 nM PPSA (Fig. 4).

The rate constant of a cross-reaction was estimated using stop-flow spectroscopy measurements monitoring $PPSA^{\bullet+}$ absorption kinetics. The estimated bimolecular rate constant of $PPSA^{\bullet+}$ reaction with HPA ($k_{12}$) was (2.5±0.2)·$10^7$ $M^{-1}$ $s^{-1}$. For HPCM, we were unable to determine bimolecular rate constant because of the fast reaction. Thus, calculated HPA self-exchange constant ($k_{11}$) was 1.8·$10^5$ $M^{-1}$ $s^{-1}$.

## The Model of Synergistic Substrate Oxidation

The peroxidase-catalyzed substrate (HPA, HPCM) oxidation can be described by simplified scheme:

$$E_{red} + H_2O_2 \rightarrow E_{ox} + H_2O \quad (7)$$

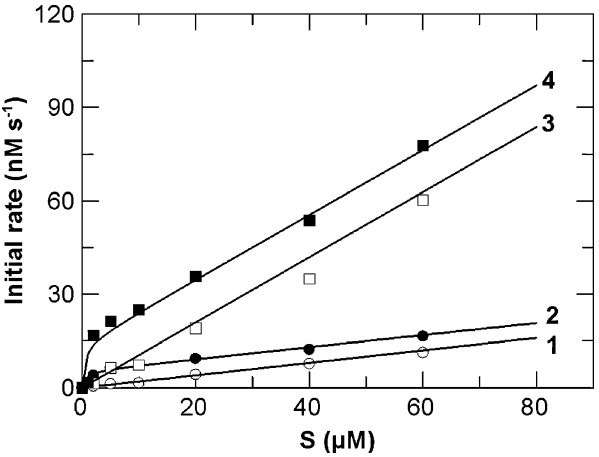


**Fig. 3** The dependence of initial oxidation rate on HPA and HPCM concentration, at pH 8.5, 25°C, 0.1 mM $H_2O_2$. (*1*) HPA without PPSA, (*2*) HPA with 3.4 nM PPSA, (*3*) HPCM without PPSA, (*4*) HPCM with 3.4 nM PPSA. Curves are the result of data fitting with a model

$$E_{ox} + S \rightarrow E_{red} + P \tag{8}$$

where $E_{red}$, $E_{ox}$, $S$, and $P$ correspond to reduced and oxidized enzyme and reduced and oxidized substrate (HPA, HPCM), respectively.

The synergistic substrate (PPSA) stimulates the oxidation of HPA and HPCM through the reactions:

$$E_{ox} + \text{PPSA} \rightarrow E_{red} + \text{PPSA}^{\cdot+} \tag{9}$$

$$\text{PPSA}^{\cdot+} + \text{S} \rightarrow \text{PPSA} + \text{P} \tag{10}$$

where PPSA and $\text{PPSA}^{\bullet+}$ correspond to reduced and oxidized PPSA. The rate constants $k_1$, $k_2$, $k_3$, and $k_4$ correspond to reactions 7–10.

To derive the initial rate expression of synergistic process, the following approximations were made: (1) the reactions of the enzyme with peroxide and electron acceptors are

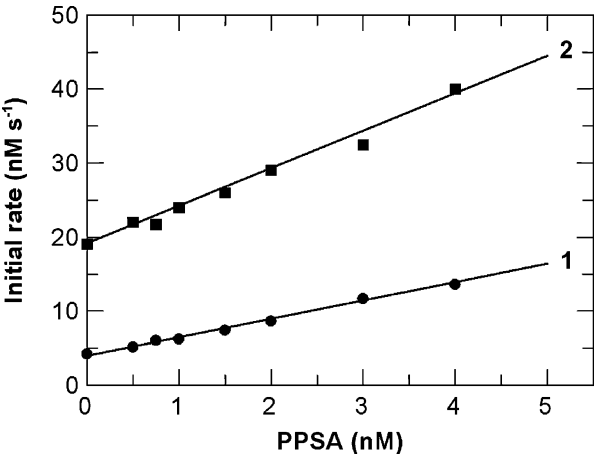


**Fig. 4** The dependence of initial oxidation rate of 20 μM HPA and HPCM on PPSA concentration, at pH 8.5, 25 °C, 0.1 mM $H_2O_2$: (*1*) 20 μM HPA with 0–4 nM PPSA, (*2*) 20 μM HPCM with 0–6.7 nM PPSA. Curves are the result of data fitting with a model

**Table 1** Experimentally determined and fitted with mathematical model rate constants of synergistic HPA, HPCM, and PPSA oxidation.

| Constant | Experimental value, $M^{-1}$ $s^{-1}$ | Fitted value, $M^{-1}$ $s^{-1}$ |
|---|---|---|
| $k_1$[a] | – | $7.1 \cdot 10^6$ |
| $k_2$ (HAA) | $(2.4 \pm 0.2) \cdot 10^3$ | $(2.5 \pm 0.3) \cdot 10^3$ |
| $k_2$ (HPCM) | $(1.4 \pm 0.2) \cdot 10^4$ | $(1.4 \pm 0.3) \cdot 10^4$ |
| $k_3$ | $(9.7 \pm 0.4) \cdot 10^7$ | $(7.2 \pm 2.1) \cdot 10^7$ |
| $k_4$ (HAA) | $(2.5 \pm 0.2) \cdot 10^7$ | $(1.7 \pm 0.4) \cdot 10^7$ |
| $k_4$ (HPCM) | – | $(4.2 \pm 0.2) \cdot 10^7$ |

[a] – reaction rate constant value taken from [1].

irreversible bimolecular processes; (2) HPA and HPCM concentrations are much larger in comparison to PPSA and do not change during measurement of the initial rate; (3) quasistationary state for the rCiP and PPSA intermediates is established. Thus, the initial rate of substrate oxidation was expressed:

$$V_s = [S]_{tot} \cdot \left(k_2 \cdot [E]_{ox} + k_4 \cdot [PPSA^{\cdot +}]\right) \tag{11}$$

where $[S]_{tot}$, $[E]_{ox}$, and $[PPSA^{\bullet +}]$ are HPA or HPCM, oxidized enzyme, and oxidized PPSA concentrations.

Steady-state $PPSA^{\bullet +}$ and $E_{ox}$ concentrations were expressed:

$$\left[PPSA^{\cdot +}\right] = k_3 \cdot [PPSA]_{tot} \cdot [E]_{ox} / \left(k_3 \cdot [E]_{ox} + k_4 \cdot [S]_{tot}\right) \tag{12}$$

$$[E]_{ox} = k_1 \cdot \left[H_2O_2\right] \cdot [E]_{tot} / \left(k_1 \cdot [H_2O_2] + k_2 \cdot [S]_{tot} + k_3 \cdot [PPSA]\right) \tag{13}$$

where $[E]_{tot}$, $[E]_{ox}$, $[PPSA]_{tot}$, [PPSA], $[S]_{tot}$, and $[H_2O_2]$ correspond to the total and oxidized enzyme, total and reduced PPSA, total substrates (HPA or HPCM), and peroxide concentrations, respectively. The derived equation was used for fitting the experimentally obtained initial rate dependences. The experimental results obtained in the absence of PPSA were fitted with $[PPSA]_{tot}=0$. Additionally, the rate constant of the $E_{ox}$ formation ($k_1=(7.1 \pm 0.1) \cdot 10^6$) was taken from the literature [1].

The analysis of the mathematical model showed that at saturated peroxide concentration the rate of synergistic process decreases when $k_4$ is less than $3 \cdot 10^5$ and $8 \cdot 10^5$ $M^{-1}$ $s^{-1}$ for HPA and HPCM, respectively. These values are two orders of magnitude less in comparison to the estimated cross-reaction (4) constants. Therefore, the fitting of experimental data was performed at fast cross-reaction ($k_4 > 10^5$ $M^{-1}$ $s^{-1}$) when the rate of chemical reaction did not limit the process. Fitted rate constants were in good agreement with those experimentally determined (Table 1).

Good fit of calculated constants supports the synergistic mechanism of rCiP-catalyzed HPA–PPSA and HPCM–PPSA oxidation. Such oxidation process could be visualized according to the following scheme (Fig. 5). The ratio of $k_3$ to $k_2$ indicates synergistic increase of HPA and HPCM oxidation rate in the presence of high active substrate [34].


**Fig. 5** Scheme of synergistic biocatalytic *N*-hydroxy compound oxidation in the presence of PPSA

**Table 2** Substrate docking energy in catalytically active state of ARP compound I/II.

| Substrate | Cluster no. | Portion of conformations in cluster, % | $\Delta G$, kJ mol$^{-1}$ |
|---|---|---|---|
| PPSA | 1 | 9.0 | −47.5 |
| | 2 | 10.5 | −45.9 |
| HPA | 1 | 66.5 | −26.9 |
| | 2 | 16.5 | −24.0 |
| HPCM | 1 | 35 | −26.3 |
| | 2 | 15 | −25.7 |

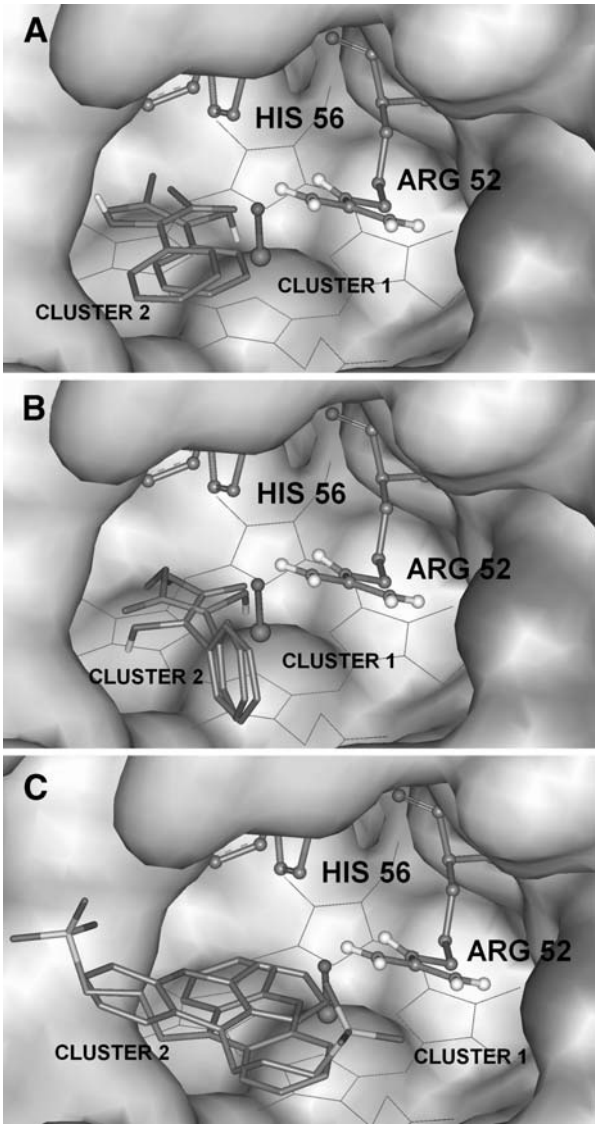


**Fig. 6** Docked conformations of HPA (**a**), HPCM (**b**), and PPSA (**c**) with lowest Gibbs energy in active site of ARP I/II

## Molecular Parameters of Substrates and Their Docking in the ARP I/II Structure

To explain the different reactivity of PPSA, HPA, and HPCM, the docking modeling in the active site of ARP I/II structure was performed. Multiple conformational clusters adopted in the active site of enzyme. Further, only numerous conformational clusters with lowest docking Gibbs free energy were analyzed (Table 2).

The docking modeling revealed that PPSA (dissociated form) exhibits the highest affinity to ARP I/II. For analysis, two distinct conformational clusters with lowest docked energy were chosen. The mean docking energies were −47.5 and −45.9 kJ $mol^{-1}$ for the first and the second cluster, respectively. In both clusters, the phenoxazine ring was located in the active site cavity coplanar to the hem plane. The data indicate that PPSA was docked at distances about 3.5 Å from ferryl oxygen accompanied by propyl sulfonic acid moiety interaction with ARG 52 and PRO 154 for the first and second cluster, respectively (Fig. 6c).

The docking data of both *N*-hydroxy derivatives indicated similar binding energy that was about 20 kJ $mol^{-1}$ higher than for PPSA (Table 2). The docking modeling indicated two possible ways of HPA arrangement in the active site of enzyme (Fig. 6a). In the first conformational cluster, N-OH moiety was at 3.8 Å and methyl group at 3.4-Å distance from ferryl oxygen atom. In the second cluster, N-OH moiety was at 5.9 Å and methyl group at 2.9-Å distance from ferryl oxygen atom. In both clusters, the benzene ring was located at the entrance of the hem cavity.

Similar results were obtained for HPCM: for first and second conformational clusters, N-OH and methyl groups were inside the active site while benzene fragment was located at

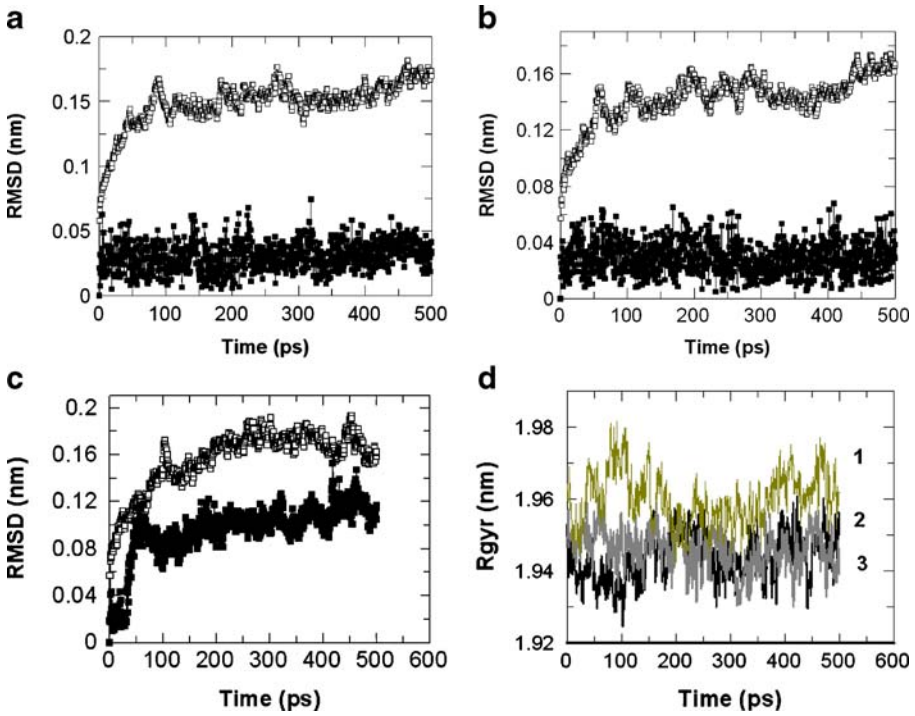


**Fig. 7** The structural stability of **a** ARP I/II-HPA, **b** ARP I/II-HPCM, and **c** ARP I/II-PPSA complexes along 0.5-ns MD simulation: calculated RMSD for ARP I/II (*empty squares*) and HPA–HPCM–PPSA (*filled squares*). **d** Calculated $R_{gyr}$ of enzyme: *curves 1*, *2*, *3* are for ARP I/II-PPSA, ARP I/II-HPA, and ARP I/II-HPCM complexes, respectively

the entrance to the hem cavity (Fig. 6b). In the first cluster, N-OH moiety was at 5.5 Å and methyl group at 4.0-Å distance from ferryl oxygen atom. In the second cluster, N-OH moiety was at 4.5 Å and methyl group at 4.2-Å distance from ferryl oxygen atom.

In order to test the stability of modeled complexes, the 0.5-ns duration molecular dynamics simulations were performed. To estimate structural change of the complexes, RMSD and $R_{gyr}$ were analyzed.

According to the RMSD parameter, HPA, HPCM, and PPSA complexes with ARP I/II were structurally stable (Fig. 7a–c). Substrate molecules stayed in the active site of enzyme during all simulation time. $R_{gyr}$ dynamics shows that ARP I/II structures in complexes with substrates remained unaltered during the overall simulation (Fig. 6d).

Several studies suggest that proton transfer may be important for peroxidase-catalyzed substrate oxidation. It was shown that proton transfer accompanies the oxidation of ferulic acid by plant peroxidase [35]. Recently, it was shown that slow proton transfer rate could be the main factor that determines low *N*-aryl hydroxamic acids and *N*-aryl-*N*-hydroxy urethanes reactivity in rCiP-catalyzed process [10, 11]. The calculations performed by Derat and Shaik also suggest that proton-coupled electron transfer is important for peroxidase-catalyzed substrate oxidation [36]. Present calculations show that substrate aril N-OH fragment is distantly located from the hem. The HPA and HPCM arrange in active site such that the methyl group is placed towards the ferryl oxygen. Thus, docking in such manner does not permit fast proton transfer to the active site of peroxidase.

## Conclusions

In this work, we demonstrate the viability of synergistic substrate oxidation. Kinetic measurements show that low reactive substrates HPA and HPCM oxidation can be stimulated using highly reactive substrate PPSA whose apparent oxidation rate constant approaches to diffusion limit of enzymic reaction. The different substrate reactivity could be explained by different docking manner in the active site of enzyme. The highly reactive PPSA exhibits the highest affinity to the enzyme active site. In comparison to PPSA, docking energies of HPA and HPCM are about 20 kJ $mol^{-1}$ higher. Thus, different affinity to active site of peroxidase is expected. Furthermore, arrangement of HPA and HPCM is unfavorable for electron transfer and proton tunneling to residues in the active site of enzyme. Docking data were confirmed using molecular dynamics simulations. The possibility to accelerate low reactive substrate oxidation rate with highly reactive substrates opens new possibilities of utilization of enzyme catalysis.

**Acknowledgements** The research was supported by the Lithuanian State Science and Studies Foundation, project BaltNano. The authors thank Dr. Arturas Ziemys for providing the ARP compound I/II structure files and helping in the computation methods and Dr. Vadimas Starikovicius for consulting and providing help in parallel computation.

## References

1. Anderson, M. B., Hsuanyu, Y., Welinder, K. G., Schneider, P., & Dunford, H. B. (1991). *Acta Chemica Scandinavica*, *45*, 1080–1086. doi:10.3891/acta.chem.scand.45-1080.
2. Yamazaki, I. (1959). In *Proceedings of the International Symposium on Enzyme Chemistry*, 224–229.
3. Pryor, W. A. (1976). In Pryor, W. A. (Ed.) *Free radicals in biology*. New York: Academic.
4. Holzenburg, A., Scrutton, N. S. (2000). *Enzyme-catalyzed electron and radical transfer*. New York: Kluwer Academic.

5. Kulys, J., & Vidziunaite, R. (2006). *Journal of Molecular Catalysis*, *37*, 79–83.
6. Goodwin, D. C., Grover, T. A., & Aust, S. D. (1996). *Chemical Research in Toxicology*, *9*, 476–483. doi:10.1021/tx950186t.
7. Call, H. P., & Mucke, I. (1997). *Journal of Biotechnology*, *53*, 163–202. doi:10.1016/S0168-1656(97)01683-0.
8. Minussi, R. C., Pastore, G. M., & Duran, N. (2007). *Bioresource Technology*, *98*, 158–164. doi:10.1016/j.biortech.2005.11.008.
9. Cambria, M. T., Minniti, Z., Librando, V., & Cambria, A. (2008). *Applied Biochemistry and Biotechnology*, *149*, 1–8. doi:10.1007/s12010-007-8100-4.
10. Kulys, J., Deussen, H. J., Krikstopaitis, K., Schneider, P., & Ziemys, A. (2001). *Monatshefte für Chemie*, *132*, 295–304.
11. Kulys, J., Deussen, H. J., Krikstopaitis, K., Lolck, R., Schneider, P., & Ziemys, A. (2001). *European Journal of Organic Chemistry*, *18*, 3475–3484. doi:10.1002/1099-0690(200109)2001:18<3475::AID-EJOC3475>3.0.CO;2-K.
12. Kulys, J., & Ziemys, A. (2001). A role of proton transfer in peroxidase-catalyzed process elucidated by substrates docking calculations. *BMC Structural Biology*, *1*, 3. doi:10.1186/1472-6807-1-3.
13. Xu, F., Kulys, J., Duke, K., Li, K., Krikstopaitis, K., Deussen, H. J., et al. (2000). *Applied and Environmental Microbiology*, *66*, 2052–2056. doi:10.1128/AEM.66.5.2052-2056.2000.
14. Indiani, Ch., Santoni, E., Becucci, M., Boffi, A., Fukuyama, K., & Smulevich, G. (2003). *Biochemistry*, *47*, 14066–14074. doi:10.1021/bi035290l.
15. Itakura, H., Oda, Y., & Fukuyama, K. (1997). *FEBS Letters*, *412*, 107–110. doi:10.1016/S0014-5793(97)00751-5.
16. Tsukamoto, K., Itakura, H., Sato, K., Fukuyama, K., Miura, S., Takahashi, S., et al. (1999). *Biochemistry*, *28*, 12558–12568. doi:10.1021/bi982925l.
17. Kulys, J., & Bratkovskaja, I. (2007). *Talanta*, *72*, 526–531. doi:10.1016/j.talanta.2006.11.011.
18. Marcus, R. A., & Sutin, N. (1985). *Biochimica et Biophysica Acta*, *811*, 265–322.
19. Kulys, J., Tetianec, L., & Ziemys, A. (2006). *Journal of Inorganic Biochemistry*, *10*, 1614–1622. doi:10.1016/j.jinorgbio.2006.05.017.
20. Frisch, M. J., Trucks, G. W., Schlegel, H. B., Scuseria, G. E., Robb, M. A., Cheeseman, J. R., et al. (2001). *Gaussian 98W*. Pittsburgh: Gaussian.
21. Goodsell, D. S., & Olson, A. J. (1990). *Proteins: Structure, Function and Genetics*, *8*, 195–202. doi:10.1002/prot.340080302.
22. Morris, G. M., Goodsell, D. S., Huey, R., & Olson, A. J. (1996). *Journal of Computer-Aided Molecular Design*, *10*, 293–304. doi:10.1007/BF00124499.
23. Morris, G. M., Goodsell, D. S., Halliday, R. S., Huey, R., Hart, W. E., Belew, R. K., et al. (1998). *Journal of Computational Chemistry*, *19*, 1639–1662. doi:10.1002/(SICI)1096-987X(19981115)19:14<1639::AID-JCC10>3.0.CO;2-B.
24. Kunishima, N., Fukuyama, K., Matsubara, H., Hatanaka, H., Shibano, Y., & Amachi, T. (1994). *Journal of Molecular Biology*, *235*, 331–344. doi:10.1016/S0022-2836(05)80037-3.
25. Berglund, G. I., Carlsson, G. H., Smith, A. T., Szoke, H., Henriksen, A., & Hajdu, J. (2002). *Nature*, *417*, 463–468. doi:10.1038/417463a.
26. Berendsen, H. J. C., van der Spoel, D., & van Drunen, R. (1995). *Computer Physics Communications*, *91*, 43–56. doi:10.1016/0010-4655(95)00042-E.
27. Lindahl, E., Hess, B., & van der Spoel, D. (2001). *Journal of Molecular Modeling*, *7*, 306–317.
28. Van Gunsteren, W. F., Billeter, S. R. Eising, A. A., Hunenberger, P. H., Kruger, P., Mark, A. E., Scott, W. R. P., Tironi, I. G. (1996). Zurich: Hochschulverlag AG an der ETH Zurich.
29. Schuettelkopf, A. W., & van Aalten, D. M. F. (2004). *Acta Crystallographica. Section D, Biological Crystallography*, *60*, 1355–1363. doi:10.1107/S0907444904011679.
30. Berendsen, H. J. C., Postma, J. P. M., Van Gunsteren, W. F., & Hermans, J. (1981). *Intermolecular forces*. Dordrecht: D Reidel.
31. Hess, B., Bekker, H., Berendsen, H. J. C., & Fraije, J. G. E. M. (1997). *Journal of Computational Chemistry*, *18*, 1463–1472. doi:10.1002/(SICI)1096-987X(199709)18:12<1463::AID-JCC4>3.0.CO;2-H.
32. Berendsen, H. J. C., Postma, J. P. M., DiNola, A., & Haak, J. R. (1984). *The Journal of Chemical Physics*, *81*, 3684–3690. doi:10.1063/1.448118.
33. Darden, T., York, D., & Pedersen, L. (1995). *The Journal of Chemical Physics*, *98*, 10089–10092. doi:10.1063/1.464397.
34. Kulys, J. (2005). *Nonlinear Analysis: Modeling and Control*, *10*, 223–233.
35. Henriksen, A., Smith, A. T., & Gajhede, M. (1999). *The Journal of Biological Chemistry*, *274*, 35005–35011. doi:10.1074/jbc.274.49.35005.
36. Derat, E., & Shaik, S. J. (2006). *Journal of the American Chemical Society*, *128*, 13940–13949. doi:10.1021/ja065058d.